Accepted Manuscript

QUARTZ : Quantitative Analysis of Retinal Vessel Topology and size
An automated system for quantification of retinal vessels morphology

M. M. Fraz[a*], R.A. Welikala[b], A.R. Rudnicka[c], C.G. Owen[c], D.P. Strachan[c], S.A. Barman[b]

[a]*School of Electrical Engineering and Computer Science, National University of Sciences and Technology, Islamabad, Pakistan*
[b]*Faculty of Science Engineering and Computing, Kingston University London, United Kingdom*
[c]*Population Health Research Institute, St. George's, University of London, United Kingdom*
[a*]moazam.fraz@seecs.edu.pk, [b]Roshan.Welikala@kingston.ac.uk, [c]arudnick@sgul.ac.uk,
[b]s.barman@kingston.ac.uk

Abstract

Retinal vessels are easily and non-invasively imaged using fundus cameras. Growing evidence including longitudinal evidence, suggests morphological changes in retinal vessels are early physio-markers of cardio-metabolic risk and outcome (as well as other disease processes). However, data from large population based studies are needed to examine the nature of these morphological associations. Several retinal image analysis (RIA) systems have been developed. While these provide a number of retinal vessel indices, they are often restricted in the area of analysis, and have limited automation, including the ability to distinguish between arterioles and venules. With the aim of developing reliable, automated, efficient retinal image analysis (RIA) software, generating a rich quantification of retinal vasculature in large volumes of fundus images, we present QUARTZ (Quantitative Analysis of Retinal Vessel Topology and size), a novel automated system for processing and analysing retinal images. QUARTZ consists of modules for vessel segmentation, width measurement and angular change at each vessel centreline pixel with sub-pixel accuracy, computing local vessel orientation, optic disc localization, arteriole/venule classification, tortuosity measurement, and exporting the quantitative measurements in various output file formats. The performance metrics of the algorithms incorporated in QUARTZ are validated on a number of publically available retinal databases (including DRIVE, STARE, CHASE_DB1, INSPIRE-AVR, and DIARETDB1). QUARTZ performs well in terms of segmentation accuracy, calibre measurement, optic disc and arteriole/venule recognition. The system provides a rich quantification of retinal vessel

morphology, which has potential medical applications in identifying those at high risk, so that prophylactic measure can be initiated before onset of overt disease.

1   Introduction

Medical imaging has revolutionized healthcare procedures, allowing professionals to detect and diagnose disease at the earliest and most treatable stages, thus improving patient outcomes with appropriate and effective care. An accurate diagnosis in medical imaging depends on the successful acquisition of the image as well as on the successful interpretation of the image. The advances in image capture hardware and the unrelenting development in computational efficiency, coupled with increasingly sophisticated image analysis and machine learning techniques, have provided the platform for acquiring minute details of biological tissues in regions such as the retina, and interpretation of the image to aid a physician in detecting possibly subtle abnormalities. With the development of digital imaging and computational efficiency, medical image processing, analysis and modelling techniques are increasingly used in all fields of medical sciences, particularly in ophthalmology and retinal image analysis.

The blood vessel structure in retinal images is unique in the sense that it is the only part of the blood circulation system that can be directly observed non-invasively and can be easily imaged using Fundus cameras. The morphological characteristics of retinal vessels are associated with cardiovascular and systemic disease. Cardiovascular disease (CVD) accounts for almost a third of deaths in both men and women, responsible for nearly 200,000 deaths in the UK per year (Statistics, 2012). Coronary heart disease (CHD), stroke and heart failure account for most of these deaths with CHD making the largest contribution. CVD is responsible for a substantial burden of morbidity and disability, accentuated by an ageing population and rising survival rates following myocardial

infarction. Diabetes is a strong risk factor for CVD both in middle and later life (SR, S, & A, 2011). The UK prevalence of diabetes, particularly type 2 diabetes (T2D) has more than doubled over 30 years (González, Johansson, Wallander, & Rodríguez, 2009; Thomas, et al., 2009). Diabetic precursors (particularly insulin resistance), as well as other blood markers, are important determinants of cardiovascular and metabolic risk (SR, et al., 2011). These precursors, along with other patient characteristics / phenotypes, are used in primary prevention to estimate future risk of cardiovascular disease, providing indications for medical / lifestyle interventions to alter disease trajectory (Collins & Altman, 2010) . Early detection and prevention of disease outcome is key, especially as morbidity and mortality are so much higher in those with CVD compared to those without. In addition to vessel features pathognomonic of overt disease (e.g., micro-aneurysms and diabetes, artery-vein nicking and hypertension), accurate measurement / monitoring of vascular morphology may be an important marker of early vascular disease, which may be important in risk prediction. Abnormalities of retinal vessels have been prospectively associated with CVD outcomes in adult life, including coronary heart disease (CHD), stroke and cardiovascular mortality (Wong, et al., 2002). In particular, narrowing of retinal arterioles has been related to CHD, and cardiovascular mortality (Wong, et al., 2002). Changes in retinal vessel calibre in later life have also been associated with established risk factors for cardiovascular disease. Narrow arterioles have been linked with the presence of hypertension and raised blood pressure (Ikram, et al., 2006; Leung, et al., 2003). Changes in retinal vessel calibre in later life have also been associated with other established risk factors for cardiovascular disease; narrow arterioles being linked to obesity and higher HDL cholesterol (Cheung, et al., 2007; Ikram, et al., 2004). Wider arterioles have been associated with higher levels of blood glucose, total cholesterol, triglycerides and inflammatory markers (Wong, et al., 2006). Associations of venular width with blood pressure have been less conclusive. Wider venules seem to be associated with diabetes, elevated glycosylated haemoglobin, lower levels of high density lipoprotein, inflammatory markers, smoking and obesity (Wang, et al., 2006; Wong, et al., 2006).

Some of these associations with vessel morphology (particularly with obesity and blood pressure) have been observed in childhood, and retinal vessel tortuosity has been associated with a number of established cardiovascular risk markers in the first decade of life (Owen, et al., 2011). This suggests life course patterning of vascular development and that retinal vessel morphology may be an important early marker of vascular health. Hence, accurate assessment of retinal vessel morphology (in both arterioles and venules) may be an important physio-marker of vascular health, which might predict those at high risk of disease in middle and later life (Abràmoff, Garvin, & Sonka, 2010).

Screening programs and large population based studies produce a large number of images to deal with, which brings specific challenges. The inter-expert variability which in-turn is the repeatability between the experts is a desirable feature. Different conclusions could be reached by two experts when they are provided with the same set of images. This may be due to the varying image conditions, difficulty related to the data analysed, observer training for this particular task or even the subjective difference in perception. Moreover, the manual segmentation, Arteriole/Venule (A/V) labelling, width marking and optic disc localization is a tedious and slow task. This inevitably results in performance decline over time for the human grader that is the challenge of intra-expert variability. Finally, with the objective of finding epidemiological associations in the images acquired from the large screening programs and population based studies, it is impossible to derive the quantitative measures of vessel morphology for each of the vessel segments in all of the retinal images. These quantitative measures may include the width measurement and the local orientation angle at each centreline pixel, the tortuosity of the vessel segment, A/V classification, the branching index of the vessel and many more.

1.1 Motivation

Epidemiological objective of retinal imaging include the following:-.

- To deliver automatic and semi-automatic image analysis for generating quantitative measures from retinal vessel morphology by establishing a common repeatable procedure, therefore increasing the reliability and performance of the analysis.

- Help to extract the quantitative measures from a large number of images acquired which can be used to find epidemiological associations.

Therefore an automated system is required which can process and analyze the large amount of data; and extract useful quantitative information from vessel morphology which helps epidemiologists and other medical experts in identifying those at high risk of disease (Trucco, et al., 2013).

There are some software systems that have been released recently for automatic and semi-automatic analysis for retinal images. This includes Retinopathy Image Search and Analysis (RISA) (Mirsharif, Tajeripour, & Pourreza) system that uses a content-based image retrieval method to perform rapid analysis and diagnosis of diabetic retinopathy from digital retinal imagery through a telemedicine model. The RoPtool (Rothaus, Jiang, & Rhiem, 2009) and RoPnet (Dashtbozorg, Mendonca, & Campilho, 2013) which are designed for the evaluation and analysis of retinopathy of prematurity in infancy. ROPnet (Dashtbozorg, et al., 2013) is an interactive tool for semi-automatic tracking of retinal vessels and computation of tortuosity index in narrow-field images, whereas RoPtool (Rothaus, et al., 2009) traces retinal blood vessels and calculates width (expressed as dilation index) and tortuosity (expressed as tortuosity index). CAIAR program (Owen, et al., 2009) developed in python and Pearl, is designed for measuring retinal vessel width and has been used to calculate tortuosity in the retinal images of school children.

Several software packages to analyse adult retinal images have been developed, including the System for the Integration of Retinal Image Understanding Services (SIRUS), Interactive Vessel Analysis (IVAN), the Vascular Assessment and Measurement Platform for Images of the Retina system (VAMPIRE), and the Singapore 'I' Vessel Assessment program (SIVA). SIVA(Vázquez, et al., 2013) developed by the Singapore Eye Research Institute is designed for extraction of the retinal vascular structure and derives quantitative measures from retinal images to describe the retinal

vessels' characteristics. IVAN (Grisan & Ruggeri, 2003) is another software tool used for obtaining clinical indexes of AVR, but the time for the analysis of a single image is approximately 20 minutes, too long to allow its use in screening studies or to become a standard in clinical practice (Huang, Zhang, & Huang, 2012). SIRIUS (Ortega, et al., 2010) is a web-based system for retinal image analysis which provides a collaborative framework for experts. SIRIUS consists of a web based client user interface, a web application server for service delivery and the service module for the analysis of retinal microcirculation using a semi-automatic methodology for the computation of the arteriolar-to-venular ratio (AVR). The RIVERS (Retinal Image Vessel Extraction and Registration System) project (Stewart & Roysam) (Tsai, et al., 2008) can also be considered as an initiative in this direction. Automated Retinal Image Analyser (ARIA) software is designed to facilitate fast, accurate and repeatable measurements of retinal vessel diameters in a variety of retinal image types. VAMPIRE (Perez-Rovira, et al., 2011) (Vascular Assessment and Measurement Platform for Images of the REtina) is a software application for semi-automatic quantification of retinal vessel properties. The system aims to provide efficient and reliable detection of retinal landmarks (optic disc, retinal zones, main vasculature), and quantify key parameters used frequently in investigative studies which includes vessel width, vessel branching coefficients and tortuosity measures. The creation of ground truths for vessel segmentation is a crucial task which entails training and skill. Live-Vessel (Kelvin, Ghassan, & Rafeef, 2007) is a semi-automatic and interactive medical image segmentation software tool for locating vessels and vascular trees in 2D color medical images.

The above discussed software packages provide a number of indices for describing the morphology of retinal vessels, they have several important limitations. In particular, they are restricted to analysis of limited areas around the optic disc, have limited automated ability to discriminate retinal arterioles from venules and provide evidence on a limited number of parameters; mainly vessel width with limited information on vessel tortuosity. Typically central retinal artery / or vein equivalent vessel widths are computed and these two summary measures do not capture variance in measures across an image, are highly dependent on the number of vessels measured and the

method of obtaining the real size. Many involve extended processing times for a single image (e.g., IVAN takes 20 minutes per image), and some charge for their use.

The rationale behind most of these systems is to focus on research and advancement of image analysis techniques and methodologies. They are not developed to run automatically on large image sets. Moreover, for retinal image analysis, there is no solution which allows epidemiologists to extract the quantitative measures from retinal vessel morphology in very large image sets automatically. In this environment, an automated computer system fulfilling the previously described features is needed. We present QUARTZ, a software system that provides epidemiologists with a framework for extracting quantitative measures of retinal vessel morphology from the images obtained from large population based studies.

Our goal is to provide fully automated software which will include:- (i) segmentation of retinal vessels, (ii) measurement of retinal vessels (including sub-pixel measures of width and tortuosity), (ii) recognition of arteriole and venule status, (iii) identification of right and left eye (by automated identification of the optic disc), (iv) derivation of information from the whole retina, not simply concentric areas centred on the optic disc.

The rest of the paper is structured as follows: Section 2 introduces the architecture and implementation of the framework. Section 3 introduces a case study for the framework, integrating the AVR computation service into it. Section 4 validates the AVR service and the framework by evaluating its performance and functionality in several real case scenarios where the application has been used. Section 5 contains some discussion about the obtained results. Section 6 offers final conclusions and future work on the web-based tool.

2 QUARTZ Overview

QUARTZ (QUantitative Analysis of Retinal vessel Topology and size) is developed to provide a tool for automated processing of large numbers of retinal images and obtain quantitative measures from vessel morphology, which will be used in epidemiological studies. It is developed with the aim to

allow multilevel data analyses allowing for multiple measures in the same individual, with right and left eye measures correlated.
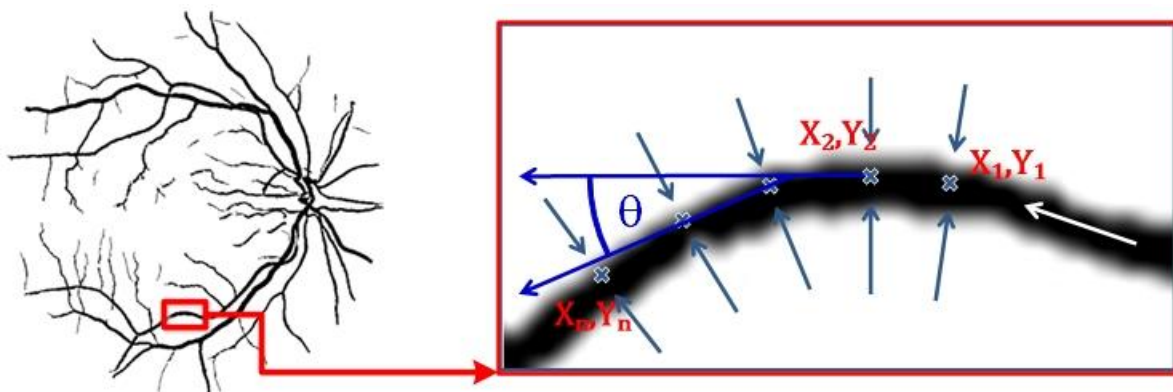
Figure 1: Quantitative measures of retinal vessel morphology

The quantitative measures derived from vessel morphology which are illustrated in Figure 1 are summarized as;

- Person / Image Identifier

- Left or right eye, which can be identified with the position of the optic disc in the macula centred retinal images.

- Classification of vessels into arterioles and venules.

- Vessel segments identification

- The centreline coordinates of vessel segments $[(X_1,Y_1) , (X_2,Y_2) ,...., (X_n,Y_n)]$

- Local orientation angle at each centreline coordinate. [θ as shown in Figure 1]

- Angular change at each vessel segment centreline coordinate, $\Delta\theta$

- Width of vessel segment at each centreline coordinate.

- Tortuosity of vessel segment

Therefore, in order to obtain the quantitative measures mentioned above, the QUARTZ software has incorporated the following modules

- Retinal blood vessel tree segmentation

- Vessel segments extraction

- Vessel width measurement

- Local angle computation

- Arteriole / Venule classification

- Optic disc localization

3 QUARTZ Algorithms

The QUARTZ software is developed in Matlab R2014a using object oriented programming (OOP). This allows the software to be structured into modules which includes blood vessel segmentation, vessel analysis module, optic disc (OD) localization module and arteriole/venule (a/v) classification component. The algorithm details of these modules are presented in this section.

3.1 Vessel Segmentation

Automated segmentation of retinal vasculature is considered as the first step in the development of computer assisted diagnostic system for eye related disease. A comprehensive review of blood vessel segmentation methodologies is available in literature (M. M. Fraz, Remagnino, et al., 2012a). Recently, a trainable COSFIRE filters is presented for retinal vessel segmentation (Azzopardi, Strisciuglio, Vento, & Petkov, 2015) and localization of bifurcations and crossovers (Azzopardi & Petkov, 2013).

The retinal vasculature is composed of arterioles and venules, appearing as piecewise linear features, with variation in width and their branches visible within the retinal image. Automatic segmentation of retinal vessels is the first step in the development of a computer aided / assisted diagnostic system for ophthalmologic studies (M.M. Fraz & Sarah A Barman, 2014; M. M. Fraz, Remagnino, et al., 2012a). There is an array of supervised and unsupervised retinal vessel segmentation algorithms developed within the research group (M. M. Fraz & Sarah A Barman, 2014; M. M. Fraz, Barman, et al., 2012; M. M. Fraz, Basit, & Barman, 2012; M. M. Fraz, Remagnino, et al., 2012b; M. M. Fraz, Rudnicka, Owen, & Barman, 2013). Supervised methods exploit some prior

labelling information to decide whether a pixel belongs to a vessel or not, while unsupervised methods perform the vessel segmentation without any prior labelling knowledge. The performance of supervised methods is better in general (M.M. Fraz & Sarah A Barman, 2014) but their prerequisite is the availability of the already classified ground truth data, which may not be available in real life applications. The ability to quantify the morphological features of the retinal vasculature for large population based studies is one of the design features of the QUARTZ software. Therefore the supervised method is not an optimal choice due to its inherent difficulties. Therefore in QUARTZ, we have implemented an unsupervised vessel segmentation algorithm based on multi-scale line detector and hysteresis morphological reconstruction.

A measure of vessel-ness for each pixel in the retinal image is computed by combining multi-scale line detection. In this procedure, the average pixel intensity is measured along lines of a particular length passing through the pixel under consideration at 12 different orientations spaced by 15 degrees each. The line with the highest average pixel intensity is selected. The line strength of a pixel is calculated by computing the difference in the average grey values of a square sub-window centred at the target pixel with the average intensity of the selected line. This concept was first introduced by (Ricci & Perfetti, 2007) and has also been employed elsewhere (M. M. Fraz, Remagnino, et al., 2012b). We have used a generalized multi-scale line detector (Nguyen, Bhuiyan, Park, & Ramamohanarao, 2012) (MLD), which uses a variable length "L_n" of aligned lines in a fixed square sub-window "W", for calculating the line strength measures for the pixels in the images containing a central vessel reflex. Figure 2 illustrates the application of the MLD on a portion of vessel exhibiting the central reflex. It can be observed in Figure 2(c) that the MLD with longer lengths "L_n" in the fixed square sub-window W (where n <= W) performs better in computing the vessel-ness measure of the pixels belonging to the central reflex but it generates false responses for background pixels which are in close vicinity to each other. The MLD with shorter lines is effective in highlighting the vessel structure but it contributes to the background noise and it does not perform well with the central reflex; as illustrated in Figure 2(b). The final measure of vessel-ness for each pixel is computed by a

linear combination of responses obtained with the MLD at different scales i.e. different line lengths, thus exploiting the strength and eliminating the limitation of each individual line detector. The size of fixed sub-window W is selected to be twice the size of a typical vessel width in the image database. We have experimentally chosen W = 25 and n = [11,15,19,23] (M. M. Fraz, Remagnino, et al., 2012b) i.e. the MLD is used at four scales Ln. In the line strength image (LSI), each value corresponds to the confidence measure of each pixel to be a part of the vessel or not. The LSI, as illustrated in Figure 3(b), is often considered as a greyscale image, where bright pixels indicate a higher probability of being a vessel pixel.
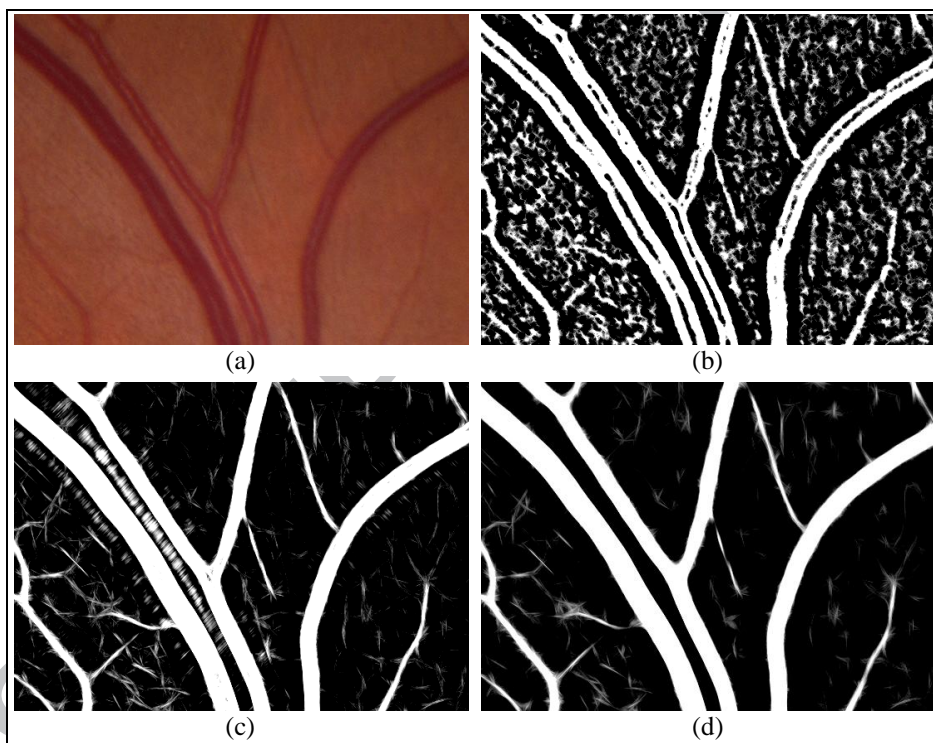
Figure 2: Line strength image; (a) Retinal image part; (b-d) Vessel-ness images; (b) MLD response with Ln ,n= 11, and (c) MLD response with Ln ,n= 23; (d) Linear combination of all MLD responses

A hysteresis thresholding based morphological reconstruction is applied to the line strength image. The details of this procedure were reported by the authors elsewhere (M. M. Fraz, Rudnicka, Owen, Strachan, & Barman, 2014). This procedure employs a bi-threshold procedure such that the LSI which is considered as an intensity image, is thresholded for two ranges of grey values, one being included in the other. The image is first segmented by a narrow threshold range which concedes

only high confidence object pixels and thus also contains many false negatives. This image is termed a marker image. The mask image is generated by applying a wide threshold range to the greyscale image. These threshold values are derived from the intensity histogram of the non-null pixels; each one of these thresholds; T1 for the marker image and T2 for the mask image, is defined as the highest intensity value such that the number of pixels with intensities above this limit is greater or equal to a predefined percentage. This percentage value is empirically selected for T1 and T2 as 90% and 95% respectively. The marker image is used as a seed for the morphological reconstruction using the mask image. Figure 3(c-e) shows the marker, mask and segmented vessels image respectively.

| (a) | (b) | (c) | (d) | (e) |
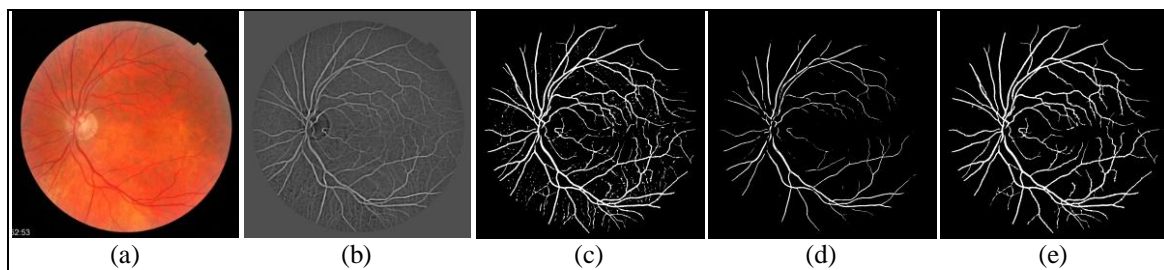
Figure 3: (a) Coloured retinal image, (b) Line strength image, (c) Marker Image, (d) Mask Image, (e) segmented vasculature

3.2   Width Measurement and Quantitative Analysis

The centrelines of the blood vessel are found by applying a morphological thinning operation to the segmented vascular tree, which iteratively removes the exterior pixels from the detected vessel thus resulting in the vessel centreline image.

The centreline image is analysed for the bifurcations and crossovers. At a bifurcation point, the blood vessel splits in to two smaller vessels. The centreline pixel at this point has three 8-connected neighbours. At a crossover point, two different blood vessels which are in general one arteriole and one venule coincide with each other at different depth levels. The centreline pixel at this point has four or more 8-connected neighbours. The bifurcations and crossovers are then removed from the centreline image thus dividing the vascular tree in to different vessel segments for further analysis. This step is necessary for two reasons. The vessels' widths are not well-defined at the branching points. Moreover, there is less amount of blood flow through the vessel after bifurcations due to a

change in vessel diameter. The vessel width measured before a significant branch point cannot be directly compared with the one measured afterwards.

The centreline image is cleaned in order to remove the centreline segments with very short (<15 pixels) length and spurs. Furthermore the distance transform of the binary vascular tree image is calculated in order to find the coarse estimate of vessel width. The distance transform gives the Euclidean distance of each vessel pixel from its closest non-vessel pixel. The estimate of vessel diameter at the widest point of the vessel segment can be found by doubling the maximum value of the distance transform along the centreline pixels. The centreline segment which is shorter in length than its estimated width will also be cleaned from the centreline image.

The local orientation of a vessel is estimated by fitting a least square cubic spline in piecewise polynomial form to the centrelines. The centripetal scheme (Lee, 1989) of defining a parametric spline curve for obtaining smooth centrelines with appropriate parameterization is utilized. The derivatives of the spline curve are evaluated to compute the vessel orientation (local angle with respect to x-axis) at centreline pixels. This scheme has also been utilized by (Bankhead, Scholfield, McGeown, & Curtis, 2012) for estimation of local vessel angles. Diameter of the vessel segment is the distance between the locations of edge points of the vessel segment orthogonal to the vessel centreline orientation, calculated at each centreline pixel.

The vessel profiles in retinal images resemble Gaussian functions. The profile of a normal blood vessel is modelled with a 2-D Gaussian function whereas the Dual-Gaussian function is used to model the profile of a vessel with a central reflex (M. M. Fraz, Remagnino, et al., 2013; M. M. Fraz, Rudnicka, et al., 2013). The 2-D model is fitted to a local section of vessel segment within a rectangular region of interest (ROI) using BFGS Quasi-Newton. The ROI along the centreline is extracted as twice the coarse estimate of vessel diameter obtained through the distance transform previously. The inflection points of the optimized Gaussian curve are calculated which corresponds with the vessel edges. The distance between the inflection points is the vessel diameter. The detailed description of the width estimation procedure is given by the authors elsewhere (M. M.

Fraz, Remagnino, et al., 2013). The vessel diameter, the local orientation angle, the vessel centrelines and the vessel edges are marked on the normal vessel segments as well as on the segments with central reflex in Figure 4.
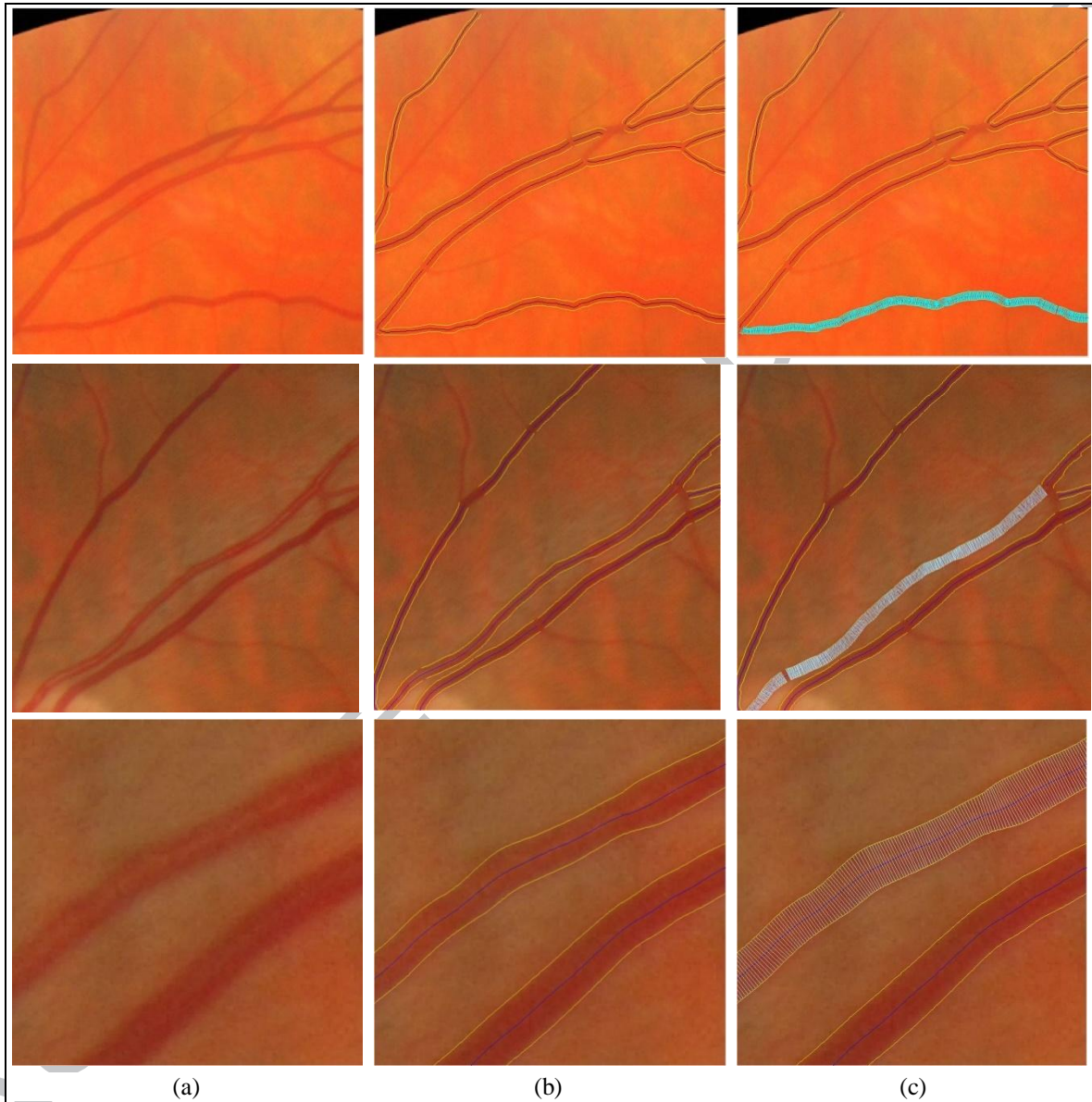
Figure 4: Demonstration of vessel diameters; (a – 1ˢᵗ column) magnified snippet of retinal image, (b – 2ⁿᵈ column) Vessel edges and centreline marking overlaid on the magnified retinal image, (c-3ʳᵈ column) Vessel width and local orientation angle marking in the vessel of interest.

3.3   Arteriole/Venule Classification

The classification of the retinal vessel is a two class classification problem where each pixel in the image either belongs to an arteriole (A) or to a venule (V). Our research group has presented an

automated method for classification of a vessel segment in to arterioles and venules based on colour features using the ensemble classifier of bagged decision trees (M. M. Fraz, et al., 2014).

For each centreline pixel in the vessel segment, the feature vector is computed using pixel based features, profile based features and vessel segment based features of the RGB and HSI colour spaces, and finally each centreline pixel is assigned an artery or vein label by a decision tree based ensemble classifier.

The pixel based features are the centreline pixel intensity values taken from the respective RGB and HSI colour channels. The profile based features are the mean and variance of the intensity values across a vessel profile for each centreline. The vessel segment based features are the mean and variance of the pixel intensities calculated for the entire vessel segment. The feature importance index and out-of-bag classification error computed during training of the classifier is helpful in determining the optimal number of features as well as the number of decision trees used to construct the ensemble classifier.

Let us consider a set of observations "x_n" from the feature vector with a known class label "y" as a training set, where y $\in$ [A, V]. The objective is to predict the class label "y" for the given observations. The classifier assigns soft labels to the centreline pixel labels, which can be regarded as a vote for the label of the complete vessel segment, and the mean of these votes is assigned as the label for the entire vessel segment. The classification of vessel segments into arterioles and venules is shown in Figure 6(a) and (b) for DRIVE and INSPIRE-AVR database images respectively, where red coloured segments are arterioles and blue coloured segments are venules.
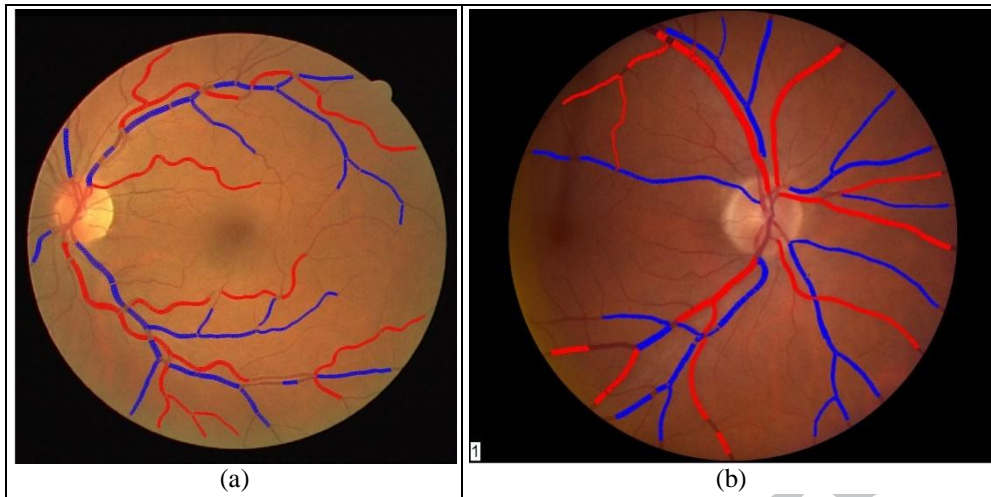
Figure 5: Classification of arterioles and venules; (a) DRIVE database Image; (b) INSPIRE-AVR database image

3.4 Optic Disc localization

The Optic Disc (OD) localization and boundary extraction method (Basit & Fraz, 2015) recently published by the authors, is based on morphological operations, regional properties and the marker controlled watershed transform. After the segmentation of the main blood vessels, the green channel of the RGB image is used for OD localization. The green channel is smoothed with a median filter and a location of maximum intensity value in this smoothed image is found. This maximum intensity value location is checked for two properties that it should not be near the boundary of the image and it must be in the neighbourhood of an extracted main blood vessel. These conditions are applied to ensure that the OD is not centred at the boundary (within 50 pixels) of the image and blood vessels enter through it. A candidate location fulfilling these conditions is regarded as a point within the OD. In case of failure, the process is repeated iteratively for the next maximum intensity value from the smoothed image until the condition is satisfied and OD location is obtained. This algorithm overcomes the problem of false OD detection and makes the method robust and efficient. The initial maxima, not satisfying the above conditions, is not within the desired location so these are eliminated repeatedly and maxima is shifts towards the OD. The location of this point is used in the subsequent boundary detection and plays an important role in the modification of the gradient image which is to be used in a watershed transformation (Gonzalez & Woods, 2002).

After the detection algorithm, the OD boundary extraction is carried out by the marker controlled watershed transformation. Two types of markers are used for modification of the gradient image: an internal marker and an external marker. The detected OD point is used as an internal marker and a circle of a predefined size is used as an external marker. The red channel of the original RGB image is more suitable for OD boundary extraction because the blood vessel effect is not so severe in this channel. Morphological operations are performed on the red channel to remove the vessel effect and large peaks. The red channel is first closed with an octagonal structuring element to further reduce the effect of vessels on the OD. Then an opening is performed with the octagonal structuring element to remove large peaks. The opened image is reconstructed to recover boundary shape and obtain the morphological gradient image of the reconstructed image. Coordinates of the detected OD point and a circle of predefined size are utilized to make a marker image. The image is reconstructed by taking the marker image and the morphological gradient as the mask. Next, the minimum imposition method modifies the gradient image which is further applied with the watershed transformation (Gonzalez & Woods, 2002) to estimate the boundary of the OD. The optic disc localization and boundary identification is illustrated in Figure 6(a) and Figure 6(b) respectively on the retinal images from DIARETDB1database.

(a)	(b)

Figure 6: (a) Optic disc localization; (b) Optic Disc boundary extraction

4   QUARTZ User Interface

The QUARTZ software is developed with the aim to extract quantifiable measures from retinal vessel morphology in larger population based epidemiological studies. Most of the functionality of the QUARTZ software can be accessed through the main screen. This section explains the interface and usability of QUARTZ.

4.1   QUARTZ Main Screen

The main screen of QUARTZ is illustrated in Figure 7. The processing options are grouped into two categories; vessel segmentation and vessel analysis. As the name indicates, the blood vessel tree is extracted in the vessel segmentation task. The vessel analysis consists of calculation of the quantifiable measures of vessel morphology, which includes vessel segment generation, measurement of diameters in the vessel segments, computing local orientation of vessel segments, optic disc localization, a/v classification and tortuosity measurement.

There is an option available to select the working directory for the images to be processed. All the images in the working directory are loaded in the software and the names of the images are shown in a selectable tabular view. This tabular view has four columns. The first column shows the index count of the retinal image, the name is shown in the second column. The last two columns named as "S" for segmentation and "W" for Analysis; depicts the processing progress of the particular retinal image in check boxes. The "S" column is checked if the segmentation result is available and the "W" column is shown checked when the vessel analysis of the image is completed. The selected retinal image can be previewed in the Image-Preview area.
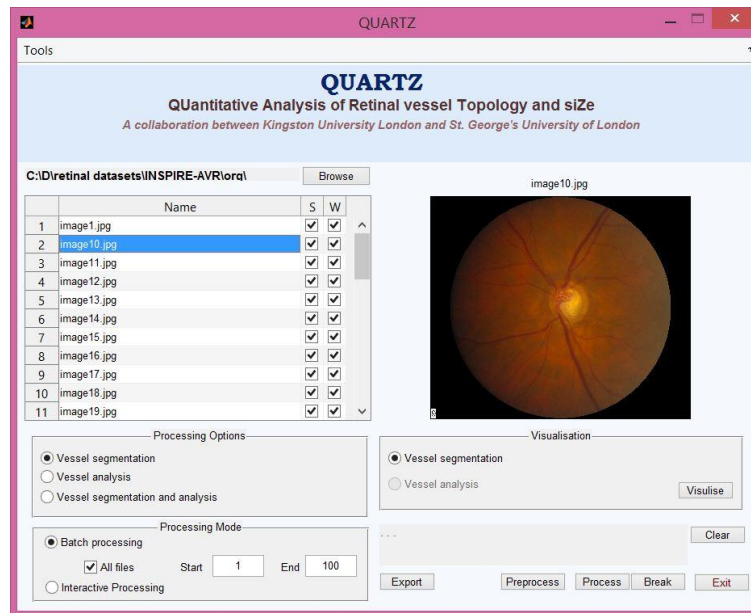
Figure 7: QUARTZ main screen

The software is designed to run in two processing modes, the batch processing mode and the interactive processing mode. In the batch processing, the selected processing option is applied to all of the images in the working directory in an automated way. The segmented vascular tree is stored as a binary image and the vessel quantification measures which are defined in section 2 are stored in a binary file. The range of retinal images can also be specified for batch processing. In the interactive mode, the chosen processing option (vessel segmentation, vessel analysis or both) is applied to the image which is selected in the selectable tabular view.

4.2   QUARTZ Configuration.

The configuration module provides the users with the functionality to specify the general working parameters for the software. The users can specify the directories for storing the extracted vascular tree, the binary file resulting after vessel analysis, and the CSV or Excel files which contain the data exported from the binary vessel analysis file. The file format for storing these files can also be specified. The region of interest in the retinal images is circular or spherical in shape therefore Field of View (FOV) masks for the retinal images are generated. These masks are generated only for the first time an image is processed and are stored in the default directory for subsequent use. The directory can be specified in the configuration module. Also there is an option available for generate

the FOV mask each time the image is processed. The quantitative measures can be exported as a CSV or Excel file, there is an option available for writing all the quantitative data in one file or generate separate files for each image under consideration. The configuration module screenshot is illustrated in Figure 8.
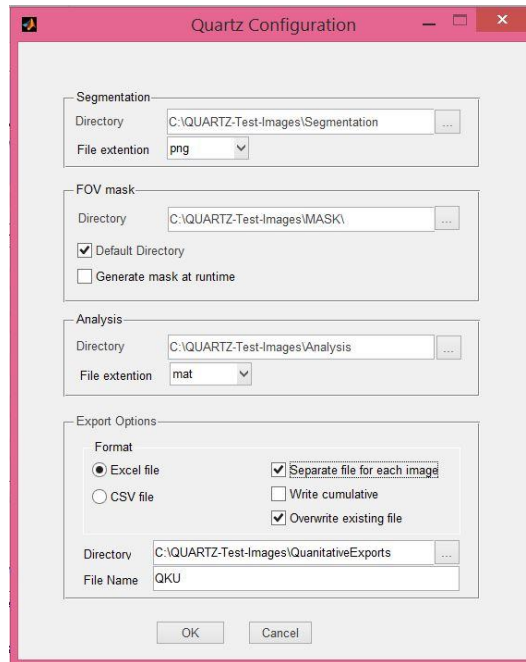
Figure 8: QUARTZ Configuration Module

4.3 Segmented Vasculature Visualization

The segmented vascular tree and the vessel analysis for the selected retinal image can also be visualized. The vessel segmentation visualization is shown in Figure 9. The segmented vascular tree can be shown as overlaid on the original RGB coloured image (Figure 9-a) or on the green channel of RGB (Figure 9-b). The segmentation overlay colour as well as the overlay opacity can also be customized for better visibility. The z-ordering of the retinal image and vascular tree can also be changed. The functionality of zoom-in, zoom-out and pan is also provided for segmentation visualization.

(a)   (b)
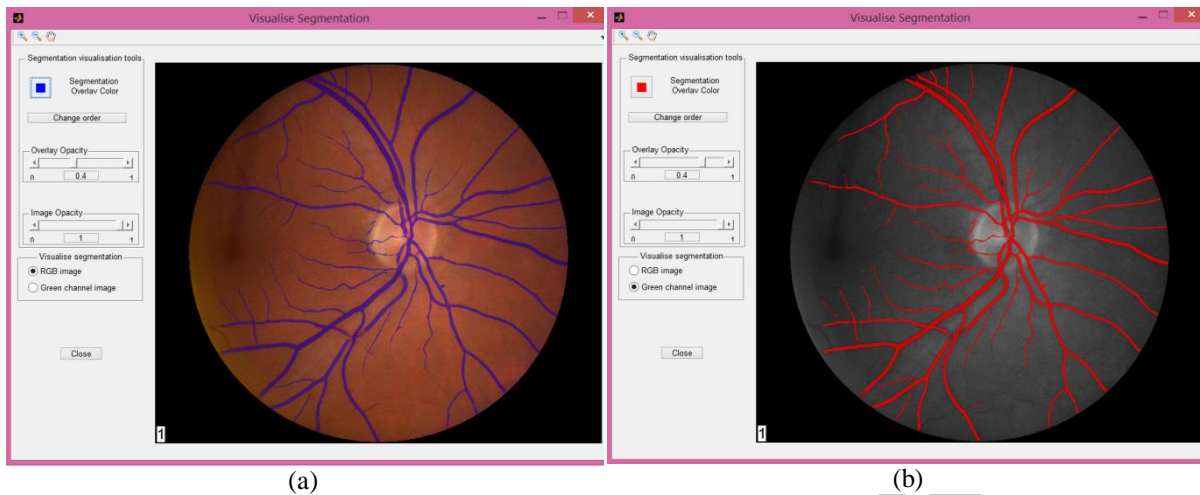
Figure 9 : Vessel segmentation visualization; (a) RGB retinal image, (b) Green Channel of RGB image

4.4 Vessel Analysis Visualization

The visualization of vessel analysis is shown in Figure 10. The marking of vessel segment edges, centrelines, diameters, labels and optic disc location can be viewed as overlaid on either the coloured RGB image or on the green channel of RGB. The visualization options are shown as highlighted in Figure 10(b), which also shows the zoomed-in view of the retinal image marked with centrelines and vessel edges.

(a)   (b)
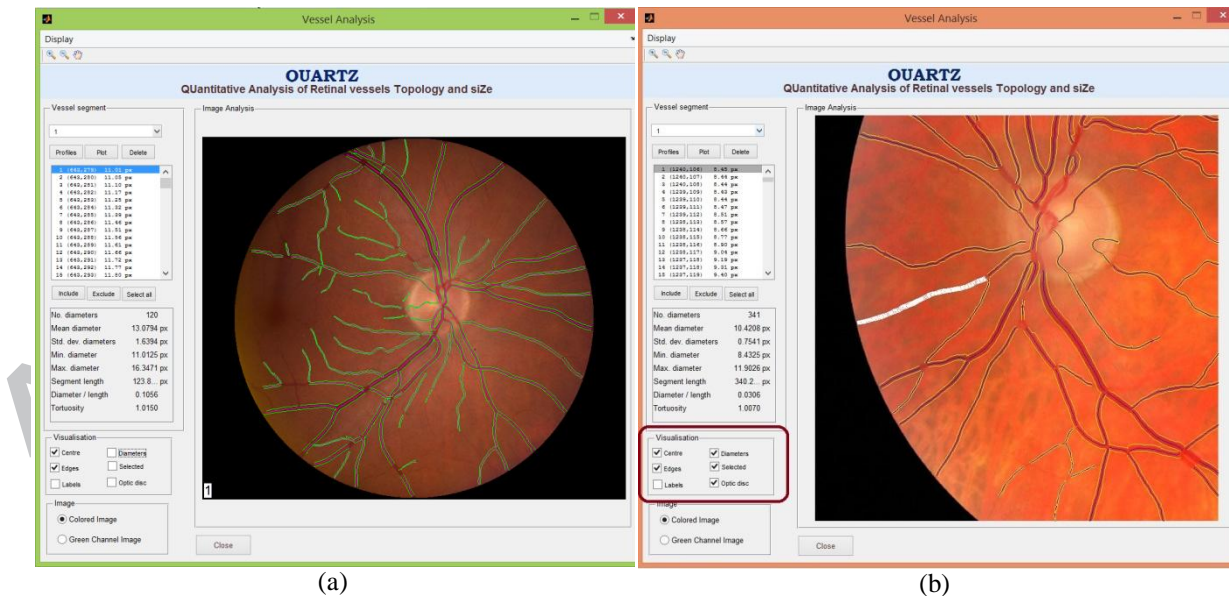
Figure 10: Vessel Analysis Visualization; (a) complete retinal image marked with centrelines and the vessel edges; (b) Magnified view of retinal image with vessel edges shown in yellow colour.

In Figure 11, the vessel segment labels, the edges, the centrelines and the diameters of a selected vessel segment are shown in the colour white. The selected diameters are shown in yellow. A list of centreline coordinates and the diameter at respective coordinates of the selected vessel is shown as highlighted in Figure 11(a).

The vessel segments can be clicked and selected in the preview area. The following properties of the selected vessel segment are shown in a table, highlighted in Figure 11(b).

- No of diameters

- Mean diameter

- Standard Deviation (SD) of diameters

- Min diameter

- Max diameter

- Segment length (in pixels)

- Diameter/Length ratio

- Vessel segment tortuosity

(a)   (b)
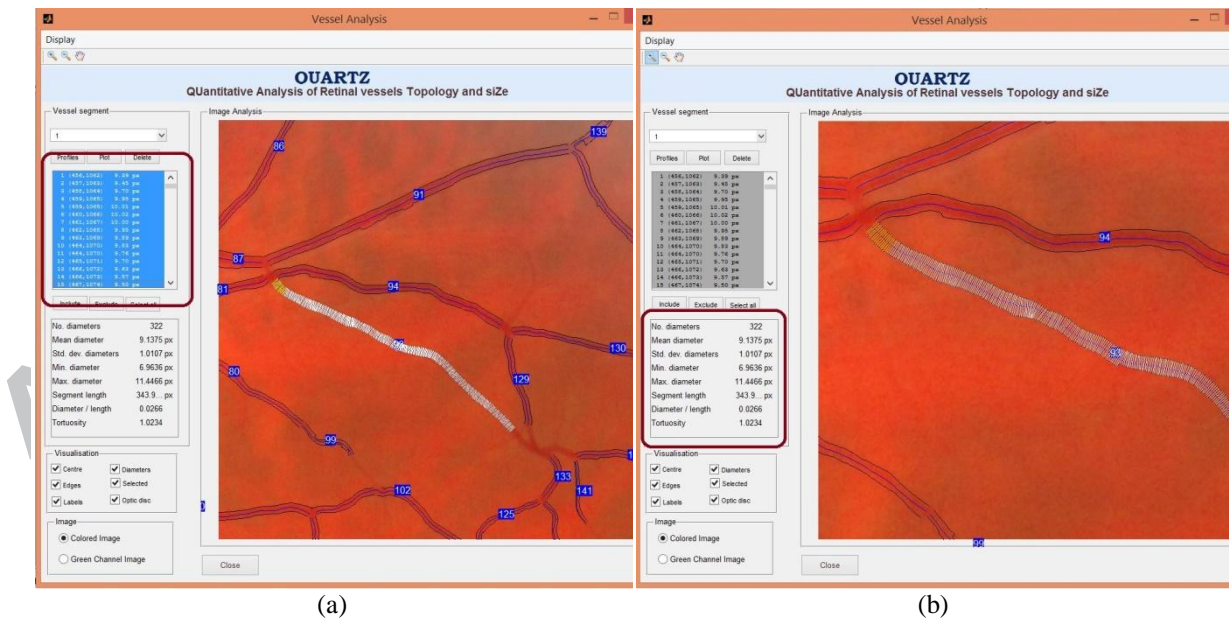
Figure 11: Vessel segment labels, diameters, edges, centrelines and selected diameters

The graph of vessel segment diameter across its length is shown in Figure 12. The vessel diameters are shown in red colour and the selected diameters in the list are visible in yellow colour.

(a) (b)
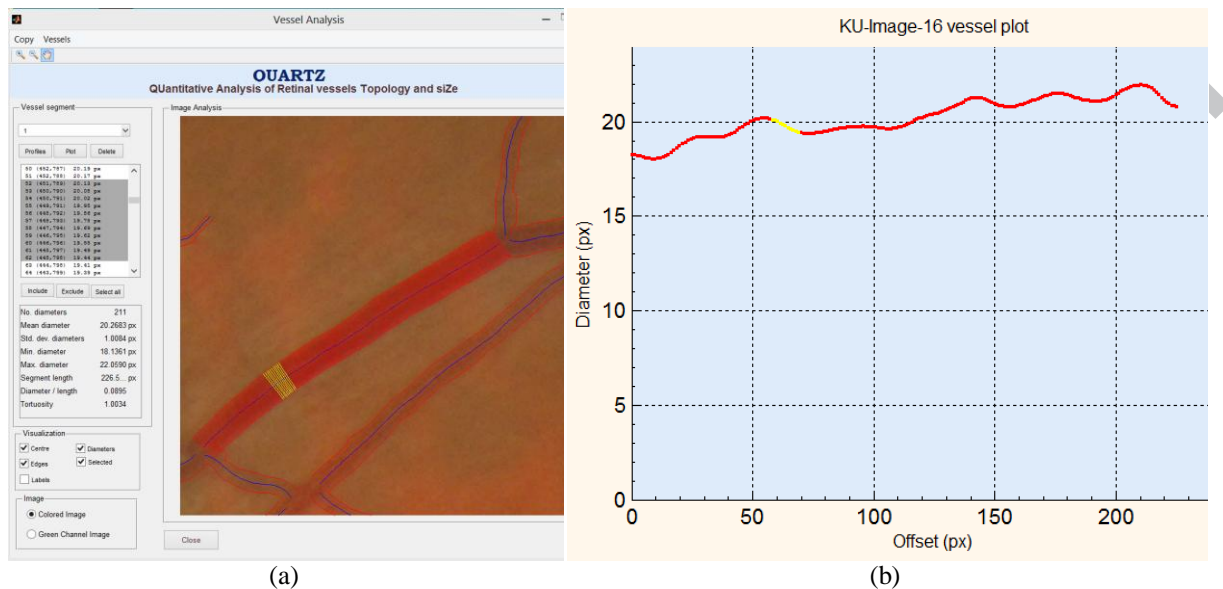
Figure 12: The plot of vessel diameter across its length; (a) selected vessel segment

The QUARTZ software system is aimed at the analysis of large data sets containing thousands of images; therefore the manual interaction with individual images is not feasible. However, the software also provides manual intervention for correction of vessel segmentation as well as for the correction of misclassified vessel segments as artery or veins.

4.5   Export of Quantitative Data

The quantification of vessel analysis can be exported as Comma Separated Values (CSV) or as a Microsoft excel sheet.

The properties related to individual vessel segments are shown in the snapshot of the CSV file in Figure 13. The vessel segment No 60 is emphasized, which is also shown as the selected vessel in Figure 12(a). The vessel segment properties include;

- Person Identifier: the Image Name

- Position of OD which in turn indicates the right/left eye

- Segment ID

- ProbA: probability that the vessel segment is an arteriole

- ProbV: probability that the vessel segment is a venule

- Number of width measures in the vessel segment

- Mean diameter of the vessel segment

- Standard deviation of vessel segment diameters

- Min diameter of vessel segment

- Max diameter of vessel segment

- Length of vessel segment measured as Euclidean distance between vessel segment end points

- Vessel segment diameter to length ratio

- Tortuosity of vessel segment

ImageName	OD X	OD Y	Segment ID	Prob A	Prob V	Number of Width Measures	Mean Width	Std Deviation of Width	Min Width	Max Width	Length (Eucleadean Distance)	Diameter/Length Ratio	Tortousity
KU-Image-64	1004	568	49	0.4333	0.5667	64	4.695596238	0.626958301	3.5288	5.8042	64.1138564	0.0732384	1.0071012
KU-Image-65	1004	568	50	0.1	0.9	59	21.6820313	1.050393653	21.068	25.508	74.21657107	0.29214542	1.0051146
KU-Image-66	1004	568	51	0	0	43	7.123391691	0.902373157	5.9232	9.3915	40.99493573	0.173762724	1.0015992
KU-Image-67	1004	568	52	0.5667	0.4333	132	5.095428323	0.802148372	4.1137	7.3358	133.9163918	0.038049325	1.0254495
KU-Image-68	1004	568	53	0	0	43	14.56600765	1.820464325	12.077	17.685	49.39647766	0.29487948	1.0062146
KU-Image-69	1004	568	54	0	1	102	21.34369856	0.559810265	20.482	22.149	115.6197817	0.184602481	1.0013866
KU-Image-70	1004	568	55	0.7	0.3	52	4.531545707	1.055913939	3.132	6.9754	53.23777983	0.085118984	1.0054975
KU-Image-71	1004	568	56	0.9333	0.0667	333	7.524161482	1.981250838	3.5157	11.854	327.4330698	0.022979235	1.0345189
KU-Image-72	1004	568	57	0.3333	0.6667	71	5.268410429	0.585452529	4.3123	6.4939	77.62029419	0.067874136	1.0095319
KU-Image-73	1004	568	58	0.9	0.1	266	5.633910836	1.107429262	3.2684	8.2645	267.7509053	0.021041613	1.02391
KU-Image-74	1004	568	59	0	0	27	11.0790179	0.962255121	9.8092	12.767	26.28852285	0.421439347	1.0140152
KU-Image-75	1004	568	60	0	1	210	20.24985604	1.024846563	18.048	21.959	225.0742943	0.089969652	1.0031284
KU-Image-76	1004	568	61	0.4	0.6	60	9.407118825	2.324242624	4.2768	11.95	61.22954708	0.153636917	1.0217453
KU-Image-77	1004	568	62	0.1333	0.8667	155	14.63766747	0.687300923	13.676	16.157	152.32774	0.096093249	1.0032346
KU-Image-78	1004	568	63	0.6333	0.3667	246	5.301018506	1.334407784	2.9949	8.6784	246.3317266	0.021519837	1.0191484
KU-Image-79	1004	568	64	0.6	0.4	80	6.655632197	1.755445195	3.7445	11.36	81.30479721	0.081860264	1.0176881
KU-Image-80	1004	568	65	0.9333	0.0667	94	14.03185509	0.780385031	13.006	16.255	91.64811632	0.153105766	1.0081655
KU-Image-81	1004	568	66	0.9667	0.0333	106	20.35564385	1.780214096	18.094	23.538	103.7930321	0.196117634	1.0042471
KU-Image-82	1004	568	67	0.8333	0.1667	120	12.98088807	2.156300501	5.5041	14.504	132.5540192	0.097929042	1.0238701
KU-Image-83	1004	568	68	1	0	188	13.67310133	0.732461374	12.252	15.695	211.1153875	0.06476601	1.0026402
KU-Image-84	1004	568	69	0.8667	0.1333	181	10.55818453	1.31461794	7.6933	13.942	186.1575091	0.056716404	1.0132676
KU-Image-85	1004	568	70	0.7	0.3	164	5.198549081	0.565438792	4.173	7.0193	167.1792998	0.031095651	1.0100447
KU-Image-86	1004	568	71	0.5667	0.4333	124	7.079844329	1.576725625	3.9524	12.099	122.5139157	0.057788083	1.0478574

Figure 13 : Vessel segment properties

Figure 14 shows the snapshot of the CSV file that contains the person identifier, segment ID, centreline coordinates, diameters and local orientation angle. The first 15 diameters of vessel segment no 60 are highlighted, which is shown in Figure 12(a). The local angle, as shown in the last column of Figure 14 is the measure of orientation of a perpendicular line passing through the vessel centreline pixel and joining two vessel edges from the x-axis. The –ve sign indicates that it is 30.06 degrees (last measure of segment 59) counter clockwise.

ImageName	Segment ID	Centerline Coordinate X	Centerline Coordinate Y	Diameter at Coordinate	Local Angle
KU-Image-16	59	1543.413549	774.3807829	12.29615054	-31.66220985
KU-Image-16	59	1543.526558	775.3594008	12.48369639	-31.33030528
KU-Image-16	59	1543.586012	776.3481515	12.62617861	-30.95340009
KU-Image-16	59	1543.588147	777.3477477	12.72055393	-30.53087502
KU-Image-16	59	1543.529196	778.3589017	12.76693422	-30.06205382
KU-Image-16	60	489.0257769	745.0048772	18.28368703	47.32825951
KU-Image-16	60	488.1371552	745.8367436	18.26583314	46.45819371
KU-Image-16	60	487.2700645	746.6726839	18.23242181	45.64630695
KU-Image-16	60	486.4225605	747.5123301	18.19054981	44.89705794
KU-Image-16	60	485.5926992	748.3553144	18.14613198	44.21456393
KU-Image-16	60	484.7785364	749.201269	18.10697674	43.60256904
KU-Image-16	60	483.9781279	750.0498261	18.07509144	43.06441932
KU-Image-16	60	483.1895297	750.9006177	18.054271	42.60304382
KU-Image-16	60	482.4107975	751.753276	18.0478754	42.22094093
KU-Image-16	60	481.6399874	752.6074332	18.05810412	41.92016911
KU-Image-16	60	480.8751551	753.4627215	18.08633417	41.70234094
KU-Image-16	60	480.1143565	754.318773	18.13347674	41.56861966
KU-Image-16	60	479.3556476	755.1752199	18.2009552	41.51971732
KU-Image-16	60	478.597084	756.0316943	18.28824428	41.5558939
KU-Image-16	60	477.8367219	756.8878283	18.38720917	41.67695709

Figure 14: Vessel segment centreline coordinate diameters and local orientation angles

5   Quantitative Analysis of Results

The results obtained evaluating the usability of QUARTZ software and validation of the algorithms are summarized in this section.

The QUARTZ software incorporates some of the retinal image processing and quantification algorithms that were previously described by our group (M.M. Fraz & Sarah A Barman, 2014; M. M. Fraz & Sarah A Barman, 2014; M. M. Fraz, Barman, et al., 2012; M. M. Fraz, Remagnino, et al., 2013; M. M. Fraz, Remagnino, et al., 2012a, 2012b; M. M. Fraz, et al., 2014). Each module and algorithm has been carefully evaluated and the validation results are presented. The performance metrics of the incorporated algorithms are evaluated and analysed on different retinal image databases available in the public domain, which includes DRIVE ("DRIVE: Digital Retinal Images for Vessel Extraction," 2004), STARE ("STARE: STructured Analysis of the Retina," 2000), CHASE_DB1 (M.M. Fraz & Barman, 2013), INSPIRE-AVR(Niemeijer, et al., 2011), and DIARETDB1(Kauppi, et al., 2007).

The accuracy of the vessel segmentation algorithm on DRIVE ("DRIVE: Digital Retinal Images for Vessel Extraction," 2004), STARE ("STARE: STructured Analysis of the Retina," 2000) and CHASE_DB1 (M.M. Fraz & Barman, 2013) is found to be 0.948, 0.953 and 0.946 respectively. The sensitivity

(detection rate) and specificity are found to be 0.740, 07554 and 0.722; and 0.980, 0.976 and 0.741 respectively. The details of the evaluation methodology are illustrated in (M. M. Fraz & Sarah A Barman, 2014; M. M. Fraz, Remagnino, et al., 2012b; M. M. Fraz, Rudnicka, et al., 2013). The average accuracy values and precision rates obtained by the algorithm are more than the 2nd human observers for the DRIVE and STARE databases. The specificity values for the algorithm are also higher than the 2nd human observer for each of the three image databases that indicates the low false positive rate of the methodology as compared with the 2nd human observer. This, in turn indicates that the algorithm has identified less numbers of background pixels or pathological area pixels as part of a vessel than the 2nd human observer.

The diameter measurement algorithm is evaluated on 1605 vessel profiles from different kinds of vessel segments in the CHASE_DB1 database (M. M. Fraz, Remagnino, et al., 2013). It includes 544 profiles from vessel segments without a central reflex, 488 profiles are from vessel segments with a central vessel reflex, 264 profiles are from the vessels with normal as well as a central reflex along their length, 309 profiles are from low contrast vessel segments with uneven background illumination. The diameters measured by the automated system are compared with the manually marked vessel widths by two human observers. The mean vessel segment diameter observed by both of the expert observers is 10.10 and 8.9 pixels respectively. The mean width computed by the methodology is approximately 7.91 pixels which align more closely with the second observer. The variance in width measured by both of the observers and estimated by the algorithm is approximately 2.0. We consider the reference standard as the average of the measures marked by two expert human observers. The mean and standard deviation of the difference in width measured by the algorithm and the reference standard is 1.62 and 1.51 respectively. It should be noted that precision in measures of width, i.e., low variance, might be more important, than absolute measures of width. Any systematic bias in measures of width may be less important, as long as clinicians measure widths consistently well, especially if detecting change in width along a vessel segment is considered important. In contrast, if measures of width fluctuate considerably due to measurement

error then changes in width along a vessel length are unlikely to be detected. The detailed evaluation of the quantification methodology is presented by the authors in (M. M. Fraz, Remagnino, et al., 2013).

The a/v classification methodology is tested on DRIVE, INSPIRE-AVR, and images from the EPIC Norfolk study (EPIC-Norfolk, 2014). The authors have reported the detailed evaluation of a/v classification on EPIC Norfolk images elsewhere (M. M. Fraz, et al., 2014). The a/v classification on the images from DRIVE and INSPIRE-AVR database are illustrated in Figure 6. The test dataset contains 2500 vessel segments from 40 colour fundus images available in the DRIVE database. The vessel segments are classified as arteriole or venule manually by expert observers. The algorithm is evaluated by using a two-fold validation methodology. The first twenty images are assigned to set S_1 and rest of the twenty images are allocated to set S_2. The classifier is then trained on S_1 and tested on S_2, followed by training on S_2 and testing on S_1. The algorithm is evaluated in terms of Detection Rate / Sensitivity ($SN_{a|v}$), Specificity ($SP_{a|v}$), Classification Accuracy ($ACC_{a|v}$), Classification Error Rate ($CER_{a|v}$), Positive Predictive Value ($PPVa|v$), Negative Predictive Value ($NPV_{a|v}$) and the Positive and Negative Likelihood Ratios ($PLR_{a|v}$ and $NLR_{a|v}$). The $ACC_{a|v}$ is measured by the ratio of the total number of correctly classified pixels (sum of true positives and true negatives) by the number of pixels under consideration in the image. $SN_{a|v}$ reflects the ability of an algorithm to detect the true positives. $SP_{a|v}$ measures the proportion of negatives that are correctly identified. $PPV_{a|v}$ or the precession rate gives the proportion of vessel pixels with correctly identified positive test results and $NPV_{a|v}$ is the proportion of vessel pixels with negative test results that are correctly identified. The predictive values depends on the percentage of a/v in the retina (prevalence), therefore the likelihood ratios ($PLR_{a|v}$ and $NLR_{a|v}$) are also computed which are not dependent on prevalence. The performance metrics are computed separately for arterioles and venules and presented in Table 1.

Table 1: Vessel classification performance metrics on DRIVE database

Measure	Arterioles		Venules	
	Tested on S1	Tested on S2	Tested on S1	Tested on S2
$SN_{a|v}$	0.9123	0.8815	0.7838	0.7652
$SP_{a|v}$	0.7758	0.7829	0.9127	0.8804
$ACC_{a|v}$	0.8487	0.8344	0.8369	0.8261
$CER_{a|v}$	0.1512	0.1682	0.1634	0.1742
$PPV_{a|v}$	0.8462	0.8342	0.8789	0.8621
$NPV_{a|v}$	0.8773	0.8542	0.8234	0.8340
$PLR_{a|v}$	3.7481	4.8341	5.5685	6.3718
$NLR_{a|v}$	0.1135	0.1403	0.2515	0.2416

The similarity in the performance metrics obtained for the sets S1 and S2 indicates the repeatability of the methodology in classification of vessels.

The working of software can be subdivided in to four modules. (1): Vessel segmentation, (2): Vessel Analysis, which further includes computation of width measurement and angular change at each vessel centreline pixel with sub-pixel accuracy, calculating local vessel orientation and tortuosity measurement, (3): optic disc localization, and (4): arteriole/venule classification. The average processing time for each module is computed on a set of 20 images randomly picked from the image dataset. The QUARTZ is evaluated for the processing time on Dell XPS 13 laptop with Corei7 processor and 8GB RAM. The measures are reported in Table 2. However, it should also be noted that the QUARTZ system is aimed at the analysis of large dataset in batch processing mode, therefore the processing time is not of very much significance.

Table 2: Average processing time for each Module is QUARTZ

S.No	Module	Average Processing Time In seconds
1	Vessel Segmentation	16.57
2	Quantitative Analysis of Segmented Vasculature • Vessel Segments Labeling • Vessel Edges and Centreline pixels identification • Vessel Width computation at each centreline pixel with sub-pixel accuracy • Tortuosity Measurement of Vessel Segment • Local angle computation at each centreline pixel	10.12
3	OD Localization	0.48
4	AV Classification	26.40

The optic disc location is used to identify the right/left eye in the macula centred retinal images. The OD localization and boundary extraction is illustrated in Figure 6. The algorithm achieves a success rate of 100% and 98.9% for DRIVE and DIARETDB1 databases respectively. The algorithm achieves an overlap of 61.88% and 54.69% for DRIVE and DIARETDB1 databases respectively. The detailed evaluation procedure for OD localization is reported by the authors elsewhere (Basit & Fraz, 2015). The quantitative comparison shows a close correlation between the automatic and manual location as well as a high spatial overlap between the OD generated by the manual method, other OD localization methodologies available in literature (Hsiao, Liu, Yu, Kuo, & Yu, 2012) and the proposed method.

6 Discussion and Conclusion

The retinal vasculature is the only part of the blood circulation system that can be directly observed non-invasively and can be easily imaged using fundus cameras. Abnormalities in morphological characteristics of arterioles and venules have been prospectively associated with a number of disease outcomes which includes hypertension, coronary heart disease, diabetes, elevated glycosylated haemoglobin, lower levels of high density lipoprotein. The assessment of the characteristics of the retinal vascular network may provide important information about early diagnosis of many systemic and vascular diseases. Epidemiologists and other medical / statistical experts study the association of retinal vessel abnormalities with other disease by examining the data gathered in the large population based studies and screening programs. The analysis of the vessel morphology and extraction of quantifiable measures from large number of images is a tedious task if performed manually.

With the aim of developing reliable, automated, efficient retinal image analysis software which can generate a rich quantification of retinal vasculature in large volumes of fundus images, we present QUARTZ (Quantitative Analysis of Retinal Vessel Topology and size), a novel automated system for processing and analysing bulk of retinal images. Several software packages to analyse adult retinal

images have been developed. While these provide several indices of retinal vessel morphology, they have several important limitations. In particular, they are restricted to analysis of limited areas around the optic disc, have limited automated ability to discriminate retinal arterioles from venules and provide evidence on a limited number of parameters; mainly vessel width with limited information on vessel tortuosity. Moreover, these packages are often semi-automated and some include extended processing times for a single image.

QUARTZ is fully automated software system that has been developed to localize and quantify the morphological characteristics of blood vessels in the retinal images, including (i) measurement of retinal vessels (including sub-pixel measures of width and tortuosity), and (ii) recognition of arteriole and venule status, (iii) automated identification of the optic disc). These measures will derive information from the whole retina, not simply concentric areas centred on the optic disc.

The automated methods for quantification of retinal vessel morphology and width may be used as an alternative to the time consuming subjective clinical evaluation for monitoring the progression of retinopathies and their association with normal and abnormal vascular patterns. This may enable early diagnosis and treatment, improving prognosis by rapid introduction of clinical health-care. QUARTZ provides quantifiable measures of retinal vessel morphology, which may enable epidemiologists / clinicians to detect the likelihood or presence of a disease by observing specific signs in combination with other external factors e.g. age symptoms and certain clinical features.

The retinal images are placed in a directory and the folder path is specified in the QUARTZ system. The system automatically loads the images from the specified directory, extract vasculature, convert it into vessel segments, classify into arteries\veins, compute local angle and tortuosity and localize optic disc. The quantitative measures can be exported as CSV files or Microsoft Excel Workbooks. The software is designed to run in two processing modes, the batch processing mode and the interactive processing mode. In the batch processing, the selected processing option is applied to all of the images in the working directory in an automated way. The number of retinal images to be processed in the working directory can also be specified. In the interactive processing mode, the

selected retinal image from the selectable tabular view can be processed according to the chosen processing option (vessel segmentation, vessel analysis or both).

QUARTZ can be used to identify early retinal vessel changes that may be physiological biomarkers of disease of cardio-metabolic risk and outcome, such coronary heart disease and stroke. Another application area is to study the effect of new therapies and drugs on disease e.g. alteration in retinal vessel measurements with a new treatments for hypertension. The quantifiable measures extracted from QUARTZ can also be used for examining the association of novel pathways in the natural history of specific disease e.g. microvascular disease pathways in stroke. It can be used to study the association between retinal vessel abnormalities and cognitive performance based on gene expression (Ding, et al., 2008). QUARTZ can assist in longitudinal studies i.e. quantitative study of the evolution and characterization of a disease, which will assist in treatment planning or investigating the response of a patient to certain treatments. The performance of the software is demonstrated to be state-of-the art in terms of segmentation accuracy, calibre measurement, optic disc and arteriole/venule recognition. In terms of automation with respect to specific large datasets, it is shown to be leading in the field.

At present, clinical detection and grading of diabetic retinopathy is largely evaluated manually by a grader who compares the patient's retinal image with a set of standard photographs and accesses the severity of retinal pathologies (abnormal blood vessel width, venous beading etc) before assigning an overall grade. An application of image processing algorithms for computer assisted analysis of digital fundus images offers a number of advantages over a manual system, including fast, timely and reliable quantification of abnormalities with a reduction of subjective human error.

Regarding future work, we aim to extend the functionality of this tool in multiple directions. The quality assessment of retinal image is an important pre-processing step for identifying those images in large datasets for which the automated analysis procedures may fail. An image is considered as inadequate when it is difficult or impossible to make a reliable clinical judgment regarding the presence or absence of disease. In the screening programs, studies (Teng, Lefley, & Claremont, 2002)

have shown that approximately 10% of the mydriatic (pupil dilation) images and 20.8% of non-mydriatic (no pupil dilation) are of inadequate quality. The major reasons for low quality images include illumination variability due to small pupil size; lack of contrast and blurriness due to poor focus, eye movement and imaging of part of the eyelid and eyelash due to blinking. Sufficient image quality is essential to ensure a reliable extraction of quantitative measures from retinal vessel morphology.

From usability point of view, an informal feedback has been gathered on the use of the QUARTZ system by epidemiologists at St. Georges University of London. The QUARTZ system has been applied to over 16000 retinal images and a more complete evaluation of the user experience of the software is planned for future work. An algorithm for change detection in OD cup-to-disc diameter ratio will be incorporated which enables this software to be used in large population based studies for glaucoma detection. Moreover, the A/V classification module will be extended towards automatic computation of Arterio-Venous Ratio. The width measurement component together with the A/V classification will be extended for automatic detection of venous beading and a/v nicking. Most importantly, the vessel segmentation algorithm will be extended such that it can detect neovascularization in the retina. This detection of formation of new vessels in the retina is a strong indicator of proliferative diabetic retinopathy (Ramlugun, Nagarajan, & Chakraborty, 2012). This enhancement will enable QUARTZ to be utilized for studying the association and linkage of different phenotypes with proliferative diabetic retinopathy in large population studies. Our research group is also working in multi-modal and hybrid registration of retinal images and more methodologies for retinal image analysis are being developed such as quantification of retinal pathologies and drusen localization, etc. These methodologies have proven very useful for clinicians and epidemiologists, thus it would be valuable to integrate them into the QUARTZ software.

References

Abràmoff, M. D., Garvin, M. K., & Sonka, M. (2010). Retinal Imaging and Image Analysis. *Biomedical Engineering, IEEE Reviews in, 3*, 169-208.

Azzopardi, G., & Petkov, N. (2013). Automatic detection of vascular bifurcations in segmented retinal images using trainable COSFIRE filters. *Pattern Recognition Letters, 34*, 922-933.

Azzopardi, G., Strisciuglio, N., Vento, M., & Petkov, N. (2015). Trainable COSFIRE filters for vessel delineation with application to retinal images. *Medical image analysis, 19*, 46-57.

Bankhead, P., Scholfield, C. N., McGeown, J. G., & Curtis, T. M. (2012). Fast Retinal Vessel Detection and Measurement Using Wavelets and Edge Location Refinement. *PLoS ONE, 7*, e32435.

Basit, A., & Fraz, M. M. (2015). Optic disc detection and boundary extraction in retinal images. *Applied Optics, 54*, 3440-3447.

Cheung, N., Saw, S. M., Islam, F. M. A., Rogers, S. L., Shankar, A., De Haseth, K., Mitchell, P., & Wong, T. Y. (2007). BMI and Retinal Vascular Caliber in Children. *Obesity, 15*, 209-209.

Collins, G. S., & Altman, D. G. (2010). An independent and external validation of QRISK2 cardiovascular disease risk score: a prospective open cohort study. *BMJ, 340*.

Dashtbozorg, B., Mendonca, A. M., & Campilho, A. (2013). An Automatic Graph-based Approach for Artery/Vein Classification in Retinal Images. *Image Processing, IEEE Transactions on, PP*, 1-1.

Ding, J., Patton, N., Deary, I. J., Strachan, M. W. J., Fowkes, F. G. R., Mitchell, R. J., & Price, J. F. (2008). Retinal microvascular abnormalities and cognitive dysfunction: a systematic review. *British Journal of Ophthalmology, 92*, 1017-1025.

. DRIVE: Digital Retinal Images for Vessel Extraction. In. (2004).

EPIC-Norfolk. (2014). European Prospective Investigation of Cancer (EPIC). In (Vol. 2014).

Fraz, M. M., & Barman, S. A. (2013). CHASE_DB1. In (Vol. 2014). London: Kingston University.

Fraz, M. M., & Barman, S. A. (2014). Computer Vision Algorithms Applied to Retinal Vessel Segmentation and Quantification of Vessel Caliber. In *Image Analysis and Modeling in Ophthalmology* (pp. 49-84): CRC Press.

Fraz, M. M., & Barman, S. A. (2014). Ensemble Classification Applied to Retinal Blood Vessel Segmentation: Theory and Implementation. In *Image Analysis and Modeling in Ophthalmology* (pp. 23-48): CRC Press.

Fraz, M. M., Barman, S. A., Remagnino, P., Hoppe, A., Basit, A., Uyyanonvara, B., Rudnicka, A. R., & Owen, C. G. (2012). An approach to localize the retinal blood vessels using bit planes and centerline detection. *Computer methods and programs in biomedicine, 108*, 600-616.

Fraz, M. M., Basit, A., & Barman, S. A. (2012). Application of Morphological Bit Planes in Retinal Blood Vessel Extraction. *Journal of Digital Imaging*, 1-13.

Fraz, M. M., Remagnino, P., Hoppe, A., Basit, A., Rudnicka, A. R., Owen, C. G., & Barman, S. A. (2013). Quantification of blood vessel calibre in retinal images of multi-ethnic school children using a model based approach. *Computerized Medical Imaging and Graphics, 37*, 60-72.

Fraz, M. M., Remagnino, P., Hoppe, A., Uyyanonvara, B., Rudnicka, A. R., Owen, C. G., & Barman, S. A. (2012a). Blood vessel segmentation methodologies in retinal images – A survey. *Computer methods and programs in biomedicine, 108*, 407-433.

Fraz, M. M., Remagnino, P., Hoppe, A., Uyyanonvara, B., Rudnicka, A. R., Owen, C. G., & Barman, S. A. (2012b). An Ensemble Classification-Based Approach Applied to Retinal Blood Vessel Segmentation. *Biomedical Engineering, IEEE Transactions on, 59*, 2538-2548.

Fraz, M. M., Rudnicka, A. R., Owen, C. G., & Barman, S. A. (2013). Delineation of blood vessels in pediatric retinal images using decision trees-based ensemble classification. *International Journal of Computer Assisted Radiology and Surgery*, 1-17.

Fraz, M. M., Rudnicka, A. R., Owen, C. G., Strachan, D. P., & Barman, S. A. (2014). Automated Arteriole and Venule Recognition in Retinal Images using Ensemble Classification. In *9th*

International Conference on Computer Vision Theory and Applications (VISAAP) (Vol. 9th). Lisbon, Portugal.

González, E. L. M., Johansson, S., Wallander, M.-A., & Rodríguez, L. A. G. (2009). Trends in the prevalence and incidence of diabetes in the UK: 1996–2005. *Journal of Epidemiology and Community Health, 63*, 332-336.

Gonzalez, R. C., & Woods, R. E. (2002). *Digital Image Processing* (Second ed.): Prentice Hall, Upper Saddle River, New Jersey.

Grisan, E., & Ruggeri, A. (2003). A divide et impera strategy for automatic classification of retinal vessels into arteries and veins. In *Engineering in Medicine and Biology Society, 2003. Proceedings of the 25th Annual International Conference of the IEEE* (Vol. 1, pp. 890-893 Vol.891).

Hsiao, H.-K., Liu, C.-C., Yu, C.-Y., Kuo, S.-W., & Yu, S.-S. (2012). A novel optic disc detection scheme on retinal images. *Expert Systems with Applications, 39*, 10600-10606.

Huang, Y., Zhang, J., & Huang, Y. (2012). An automated computational framework for retinal vascular network labeling and branching order analysis. *Microvascular Research, 84*, 169-177.

Ikram, M. K., de Jong, F. J., Vingerling, J. R., Witteman, J. C. M., Hofman, A., Breteler, M. M. B., & de Jong, P. T. V. M. (2004). Are Retinal Arteriolar or Venular Diameters Associated with Markers for Cardiovascular Disorders? The Rotterdam Study. *Investigative Ophthalmology & Visual Science, 45*, 2129-2134.

Ikram, M. K., Witteman, J. C. M., Vingerling, J. R., Breteler, M. M. B., Hofman, A., & de Jong, P. T. V. M. (2006). Retinal Vessel Diameters and Risk of Hypertension. *Hypertension, 47*, 189-194.

Kauppi, T., Kalesnykiene, V., Kamarainen, J.-K., Lensu, L., Sorri, I., Raninen, A., Voutilainen, R., Pietilä, J., Kälviäinen, H., & Uusitalo, H. (2007). DIARETDB1 diabetic retinopathy database and evaluation protocol. In *Medical Image Understanding and Analysis (MIUA2007)* (pp. 61-65). Aberystwyth, Wales, UK.

Kelvin, P., Ghassan, H., & Rafeef, A. (2007). Live-vessel: extending livewire for simultaneous extraction of optimal medial and boundary paths in vascular images. In *Proceedings of the 10th international conference on Medical image computing and computer-assisted intervention*. Brisbane, Australia: Springer-Verlag.

Lee, E. T. Y. (1989). Choosing nodes in parametric curve interpolation. *Computer-Aided Design, 21*, 363-370.

Leung, H., Wang, J. J., Rochtchina, E., Tan, A. G., Wong, T. Y., Klein, R., Hubbard, L. D., & Mitchell, P. (2003). Relationships between Age, Blood Pressure, and Retinal Vessel Diameters in an Older Population. *Investigative Ophthalmology & Vis, 44*, 2900-2904.

Mirsharif, Q., Tajeripour, F., & Pourreza, H. Automated characterization of blood vessels as arteries and veins in retinal images. *Computerized Medical Imaging and Graphics*.

Nguyen, U. T. V., Bhuiyan, A., Park, L. A. F., & Ramamohanarao, K. (2012). An effective retinal blood vessel segmentation method using multi-scale line detection. *Pattern Recognition*.

Niemeijer, M., Xiayu, X., Dumitrescu, A. V., Gupta, P., van Ginneken, B., Folk, J. C., & Abramoff, M. D. (2011). Automated Measurement of the Arteriolar-to-Venular Width Ratio in Digital Color Fundus Photographs. *Medical Imaging, IEEE Transactions on, 30*, 1941-1950.

Ortega, M., Barreira, N., Novo, J., Penedo, M. G., Pose-Reino, A., & Gómez-Ulla, F. (2010). Sirius: A web-based system for retinal image analysis. *International journal of medical informatics, 79*, 722-732.

Owen, C. G., Rudnicka, A. R., Mullen, R., Barman, S. A., Monekosso, D., Whincup, P. H., Ng, J., & Paterson, C. (2009). Measuring Retinal Vessel Tortuosity in 10-Year-Old Children: Validation of the Computer-Assisted Image Analysis of the Retina (CAIAR) Program. *Investigative Ophthalmology & Visual Science, 50*, 2004-2010.

Owen, C. G., Rudnicka, A. R., Nightingale, C. M., Mullen, R., Barman, S. A., Sattar, N., Cook, D. G., & Whincup, P. H. (2011). Retinal Arteriolar Tortuosity and Cardiovascular Risk Factors in a

Multi-Ethnic Population Study of 10-Year-Old Children; the Child Heart and Health Study in England (CHASE). *Arteriosclerosis, Thrombosis, and Vascular Biology, 31*, 1933-1938.

Perez-Rovira, A., MacGillivray, T., Trucco, E., Chin, K. S., Zutis, K., Lupascu, C., Tegolo, D., Giachetti, A., Wilson, P. J., Doney, A., & Dhillon, B. (2011). VAMPIRE: Vessel assessment and measurement platform for images of the Retina. In *Engineering in Medicine and Biology Society,EMBC, 2011 Annual International Conference of the IEEE* (pp. 3391-3394).

Ramlugun, G. S., Nagarajan, V. K., & Chakraborty, C. (2012). Small retinal vessels extraction towards proliferative diabetic retinopathy screening. *Expert Systems with Applications, 39*, 1141-1146.

Ricci, E., & Perfetti, R. (2007). Retinal Blood Vessel Segmentation Using Line Operators and Support Vector Classification. *Medical Imaging, IEEE Transactions on, 26*, 1357-1365.

Rothaus, K., Jiang, X., & Rhiem, P. (2009). Separation of the retinal vascular graph in arteries and veins based upon structural knowledge. *Image and Vision Computing, 27*, 864-875.

SR, S., S, K., & A, T. (2011). Diabetes Mellitus, Fasting Glucose, and Risk of Cause-Specific Death. *New England Journal of Medicine, 364*, 829-841.

. STARE: STructured Analysis of the Retina. In. (2000).

Statistics, O. f. N. (2012). Deaths Registered in England and Wales in 2010, by Cause. In (Vol. April 2014).

Stewart, C. V., & Roysam, B. RIVERS; Retinal Image Vessel Extraction and Registration System http://cgi-vision.cs.rpi.edu/cgi/RIVERS/index.php. In.

Teng, T., Lefley, M., & Claremont, D. (2002). Progress towards automated diabetic ocular screening: A review of image analysis and intelligent systems for diabetic retinopathy. *Medical and Biological Engineering and Computing, 40*, 2-13.

Thomas, M. C., Hardoon, S. L., Papacosta, A. O., Morris, R. W., Wannamethee, S. G., Sloggett, A., & Whincup, P. H. (2009). Evidence of an accelerating increase in prevalence of diagnosed Type 2 diabetes in British men, 1978–2005. *Diabetic Medicine, 26*, 766-772.

Trucco, E., Ruggeri, A., Karnowski, T., Giancardo, L., Chaum, E., Hubschman, J. P., al-Diri, B., Cheung, C. Y., Wong, D., Abràmoff, M., Lim, G., Kumar, D., Burlina, P., Bressler, N. M., Jelinek, H. F., Meriaudeau, F., Quellec, G., MacGillivray, T., & Dhillon, B. (2013). Validating Retinal Fundus Image Analysis Algorithms: Issues and a Proposal. *Investigative Ophthalmology & Visual Science, 54*, 3546-3559.

Tsai, C. L., Madore, B., Leotta, M. J., Sofka, M., Yang, G., Majerovics, A., Tanenbaum, H. L., Stewart, C. V., & Roysam, B. (2008). Automated Retinal Image Analysis Over the Internet. *Information Technology in Biomedicine, IEEE Transactions on, 12*, 480-487.

Vázquez, S. G., Cancela, B., Barreira, N., Penedo, M. G., Rodríguez-Blanco, M., Pena Seijo, M., Tuero, G. C., Barceló, M. A., & Saez, M. (2013). Improving retinal artery and vein classification by means of a minimal path approach. *Machine Vision and Applications, 24*, 919-930.

Wang, J. J., Taylor, B., Wong, T. Y., Chua, B., Rochtchina, E., Klein, R., & Mitchell, P. (2006). Retinal Vessel Diameters and Obesity: A Population-Based Study in Older Persons. *Obesity, 14*, 206-214.

Wong, T. Y., Islam, F. M. A., Klein, R., Klein, B. E. K., Cotch, M. F., Castro, C., Sharrett, A. R., & Shahar, E. (2006). Retinal Vascular Caliber, Cardiovascular Risk Factors, and Inflammation: The Multi-Ethnic Study of Atherosclerosis (MESA). *Investigative Ophthalmology & Visual Science, 47*, 2341-2350.

Wong, T. Y., Klein, R., Sharrett, A. R., Duncan, B. B., Couper, D. J., Tielsch, J. M., Klein, B. E. K., & Hubbard, L. D. (2002). Retinal Arteriolar Narrowing and Risk of Coronary Heart Disease in Men and Women. *JAMA: The Journal of the American Medical Association, 287*, 1153-1159 http://jama.ama-assn.org/content/1287/1159/1153.abstract.

Highlights

Automated system for interactive / batch processing of large number of retinal images

Extract useful quantifiable measurements of retinal vessel morphology

Modules for vessel segmentation, width, tortuosity measurement at sub-pixel accuracy

Components for Artery / Vein classification, OD localization, tortuosity measurement

Epidemiological study of association of vessel morphology with disease precursor